Heliyon 10 (2024) e33739

Contents lists available at ScienceDirect

Heliyon

journal homepage: www.cell.com/heliyon

Research article

Alveolar macrophages and monocyte subpopulations during *Plasmodium berghei* NK65 experimental malaria-associated acute respiratory distress syndrome

Flaviane Vieira-Santos [a], Ramayana Morais de Medeiros Brito [a], Camila de Almeida Lopes [a], Thais Leal-Silva [a], Jorge Lucas Nascimento Souza [a], Chiara Cássia Oliveira Amorim [a], Ana Cristina Loiola Ruas [a], Luiza de Lima Silva Padrão [a], Lucas Kraemer [a], Fabrício Marcus Silva Oliveira [a], Marcelo Vidigal Caliari [b], Remo Castro Russo [c], Ricardo Toshio Fujiwara [a], Luisa Mourão Dias Magalhães [a], Lilian Lacerda Bueno [a,*]

[a] *Laboratory of Immunobiology and Control of Parasites, Department of Parasitology, Institute of Biological Sciences, Federal University of Minas Gerais, Belo Horizonte, Brazil*
[b] *Laboratory of Protozooses, Department of General Pathology, Institute of Biological Sciences, Universidade Federal de Minas Gerais, Belo Horizonte, Brazil*
[c] *Laboratory of Pulmonary Immunology and Mechanics, Department of Physiology and Biophysics, Institute of Biological Sciences, Federal University of Minas Gerais, Belo Horizonte, Brazil*

ARTICLE INFO

Keywords:
Alveolar macrophages
Plasmodium berghei NK65-NY
Acute respiratory distress syndrome
Monocytes
Inflammation

ABSTRACT

Alveolar macrophages (AM) and monocytes (MO) are myeloid cells that play a substantial role in the development and establishment of the innate and adaptive immune response. These cells are crucial for host defense against various pathogens, but their role in malaria is poorly understood. Here, we characterize the dynamics of AMs and recruited leukocytes subpopulations in the airways during experimental *Plasmodium berghei* NK65-NY (PbNK65). We show that PbNK65 infection induces an increased pulmonary vascular permeability that provides Ly6C^{low} MOs, neutrophils (NEU), CD4^{+} and CD8^{+} lymphocytes in the airways. This inflammatory environment resulted in an increase in the population and alteration of the activation state of the AMs. Taken together, the data presented provide new insights into airway inflammation associated with pulmonary malaria.

1. Introduction

Malaria remains a significant global health problem. In 2022, there were an estimated 249 million cases of malaria that resulted in 608,000 deaths worldwide [1]. Malaria-associated acute lung injury/acute respiratory distress syndrome (MA-ALI/ARDS) is one of the main clinical complications of malaria, which predominantly affects adults and often leads to rapid deterioration and poor prognosis [2].

* Corresponding author.
E-mail address: llbueno@icb.ufmg.br (L.L. Bueno).

https://doi.org/10.1016/j.heliyon.2024.e33739
Received 12 September 2023; Received in revised form 20 May 2024; Accepted 26 June 2024
Available online 2 July 2024

The recognition of components released by the parasite, such as hemozoin, induces an intracellular signaling cascade triggering the production of inflammatory cytokines such as TNF-α, IL-1β and IL-12, as well as the release of chemokines, which attract leukocytes to eliminate the parasite [3–6]. However, the exacerbated pulmonary inflammatory response results in the breakdown of the alveolar-capillary membrane integrity with consequent thickening of the interalveolar septum and hypoxemia [7–9]. This intense inflammation plays a critical role in ALI development [10,11]. Although $CD8^+$ T cells play a key role in the development of MA-ALI/ARDS, the immune response triggered during the infection is quite complex and involves various cell types, including monocytes, macrophages and neutrophils [4–6,12,13].

Alveolar macrophages (AMs), the lung resident macrophages, are the first-line defenders of the alveoli and airways [14,15]. Under homeostatic conditions, AMs continuously regulate the alveolar environment by phagocytosing inhaled particles, pathogens, and apoptotic cells. AMs also play a critical role in the maintenance of lung physiology by uptake and recycling of surfactant in alveoli, which reduces surface tension at the air-liquid interface and prevents alveolar collapse [16–20]. However, when homeostasis is disturbed, AMs can transition to a pro-inflammatory state, secreting inflammatory cytokines and chemokines that attract and recruit leukocytes to the lungs [14–16,21]. Nevertheless, the role of AMs in MA-ALI/ARDS remains insufficiently understood [22–25].

In this sense, our study aims to investigate the AMs and infiltrated leukocytes dynamics in the airways during the PbNK65-NY severe malaria model. Our findings review that PbNK65 infection promotes increased vascular permeability in the lungs, leading to transient $Ly6C^+$ MOs accumulation, concomitantly with the influx of $CD4^+$ and $CD8^+$ lymphocytes, as well as increase and alteration of activation state of the AMs in the airways. This inflammatory scenario results in severe and irreversible pulmonary dysfunction. Collectively, our results offer new insight into understanding lung inflammation in the PbNK65-NY severe malaria model, shedding light on the intricate mechanisms underlying this debilitating condition and potentially offering new avenues for therapeutic interventions.

2. Materials and methods

2.1. Ethical statements

All experiments conducted in this study were approved by the Ethics Committee for Animal Experimentation (CEUA) of the Federal University of Minas Gerais (UFMG), Brazil, under protocol n. 114/2019, according to the Brazilian College of Animal Experimentation (COBEA) guidelines and regulations. All efforts were made to minimize animal suffering.

2.2. Mice, parasites and experimental infections

Seven-week-old male specific pathogen–free (SPF) C57BL/6j mice were obtained from the Central Animal Facility of the Federal University of Minas Gerais, Brazil. During the experimental period, mice were organized into four groups, being: three groups of eight animals/group (infected groups) and one group of six animals (control group). All mice were maintained at the Animal Facility of the Department of Parasitology of the Federal University of Minas Gerais under controlled temperature conditions (24 ± 1 °C) and lighting (12-h light-dark cycle), and fed with a commercial chow (Nuvilab Cr-1, Nuvital Nutrients, Brazil) *ad libitum* and had unrestricted access

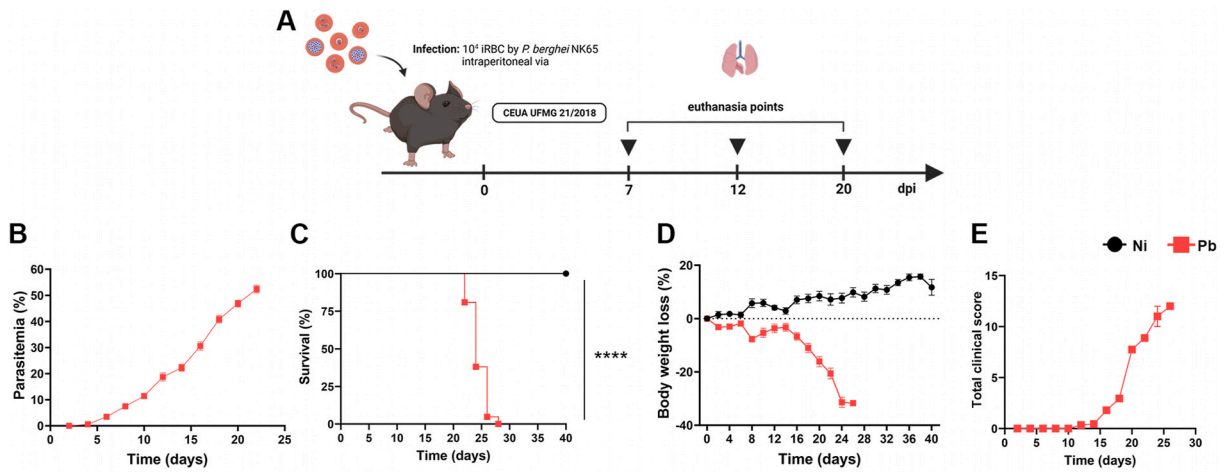

Fig. 1. Clinical parameters and peripheral inflammation profile during *P. berghei* NK65 infection. (A) Experimental design; C57BL/6j mice were infected with the New York line of *P. berghei* NK65 (inoculum of 10^4 iRBCs) and euthanized at 7-, 12- and 20-dpi. (B) Parasitemia levels, analyzed with stained blood smears from the mice tail vein. (C) Survival rate. (D) Body weight loss. (E) Clinical score (n = 6 for control, and n = 21 for infected mice). Gehan-Breslow-Wilcoxon test was used in survival analysis. Two-way ANOVA test followed by multiple comparisons test was used on body weight loss data. The data presented here is representative of two independent experiments. *$p < 0.05$, **$p < 0.01$, ***$p < 0.001$, and ****$p < 0.0001$.

to filtered water.

Cryopreserved stocks of the New York line of PbNK65-iRBCs were thawed, transferred through donor BALB/c mice, and used between passages 3–6. Donor mice were monitored daily and exsanguinated for experimental infection in ascending periods of parasitemia. Mice were infected by intraperitoneal (i.p.) injection with phosphate-buffered saline (PBS) containing 1×10^4 PbNK65 iRBCs and euthanized at 7-, 12- and 20-days post-infection (dpi). Non-infected animals were mock inoculated with 100 μL of PBS (Fig. 1A). Parasitemia was monitored by stained blood smears from the mice tail vein, and the percentage of iRBC was calculated based on the total number of non-infected red blood cells.

The parasitemia assessment was performed through analysis of air-dried blood smears, fixed with methanol, and stained with giemsa. The readings were performed in a specific optic with a comprehension objective (1,000X). Parasitemia was determined by counting the number of iRBCs out of 1000 RBCs in total. Parasitemia was expressed as a percentage of infected red blood cells.

2.3. Clinical score and survival

To evaluate the course of infection, survival, parasitemia and clinical parameters of the animals were evaluated daily. All animals were followed for up to 40 days and disease progression was scored, according to a methodology adapted from Ref. [26]: piloerection (PE), shivering (Sh), abnormal breathing (AB), trunk curvature (TC), dehydration (D), paralysis (P) to calculate a clinical disease severity score. Disease scores were given as 0 (absent) or 1 (present) for PE, Sh, AB and TC and 0 (normal), 1 (intermediate) or 2 (most severe) for the other parameters. The total clinical score was calculated using the following formula: (PE + Sh + AB + TC) +3*(D + P). The day of spontaneous death for each animal was computed and the survival curve was constructed according to Kaplan-Meyer. For comparative analysis between groups, the Log-Rank test was used.

2.4. Evans blue dye perfusion for vascular leakage

Vascular leakage in mice was determined using Evans blue dye staining, as previously reported, with minor modifications [27,28]. Briefly, mice were intravenously injected with 100 μL of a 2 % solution in PBS of the plasma marker Evans blue. One hour later, mice were exsanguinated under anesthesia. The heart left ventricle was perfused with 20 mL of PBS to remove the intravascular-localized dye. After lung tissue was excised and cleaned of connective tissue, Evans blue was extracted by incubation in formamide (1 mL formamide/100 mg of tissue) at 60 °C for 24 h. The samples were centrifuged at 12,000×*g*, 20 min at 20 °C and the supernatants were used to quantify the absorbance of Evans blue at a wavelength of 620 nm by a VersaMax ELISA microplate reader (Molecular Devices, USA).

2.5. Bronchoalveolar lavage (BAL) and protein quantification

The bronchoalveolar lavage was performed as previously described [29]. To quantify the total protein in BAL, the BCA Protein Assay kit (Thermo Scientific, USA) was used to measure possible protein leakage into the airways, as previously described [30]. The extent of alveolar hemorrhage was assessed by the amount of hemoglobin (Hb) detected in the BAL supernatant using the Drabkin method according to the manufacturer's instructions (Bioclin, Brazil). The hemoglobin concentration in the samples was determined spectrophotometrically by measuring absorbance at 540 nm. Hemoglobin content was expressed as g/dL of Hb per mL of BAL.

2.6. Multiparametric flow cytometry

Multiparametric flow cytometric analyses were performed in BAL of non-infected and infected mice with 12 and/or 20 dpi to characterize myeloid and lymphoid cell populations. Flow cytometry was performed as previously described [29]. Firstly, cells were incubated with brefeldin (BD Biosciences®) at a concentration of 1 μg/mL at 5 % CO_2 for 4 h at 37 °C. After brefeldin incubation, red blood cells were lysed with ACK for 5 min (1x, if necessary). After the lysis cycle, cells were washed with PBS and centrifuged at 300×*g*, 8 min, 4 °C.

Cells were counted in Neubauer chamber using Trypan blue and incubated with the viability dye (BD Bioscience®, Fixable viability stain 700, 1:1000) for 10 min at 4 °C. After incubation, and cells were washed by centrifugation at 300×*g*, 8 min, 4 °C with PBS and incubated with a 50 μL mix of surface antibodies containing 10 % control mice serum for 15 min at 4 °C (Supplementary Table 1) and washed with PBS by centrifugation at 300×*g*, 8 min, 4 °C. Samples were then fixed with 2 % of paraformaldehyde (PFA) for 20 min at room temperature (RT). After fixation, cells were washed twice with PBS and permeabilized by incubation for 15 min with a 0.5 % saponin solution and proceeded to intracellular staining (Supplementary Table 1). 50 μL of intracellular antibody mix were incubated for 30 min at RT in the dark. After intracellular staining, cells were washed twice with 0.5 % saponin solution and resuspended in PBS. Samples were acquired using the LSR Fortessa (BD Biosciences, USA) and analyzed with FlowJo software (Tree Star, Ashland, OR).

Data analysis was followed by dimensionality reduction and visualization by t-Distributed Stochastic Neighbor Embedding (tSNE), diffusion map and heatmap using Cytofikit 2 [31]. Clustering was performed by guided FlowSom. Each experimental group in tSNE analysis represents six mice with the input of the same number of cells. A heatmap of cytokines was made using the ClustVis web tool [32].

2.7. Histopathological analysis

Lungs from infected and non-infected mice were removed and weighed. After, the organs were fixed in 10 % formalin solution, gradually dehydrated in ethanol before being diaphanized in xylol, and included in paraffin blocks that were cut at 4 μm thick and fixed on the histopathological slides stained with hematoxylin and eosin (HE) for histopathological, semiquantitative morphometric analysis. Lesions displayed in lung parenchyma were described in terms of lesion intensity, inflammation, and vascular phenomena.

For lung lesions score [33], 10 random images were captured per animal with a 20× magnification objective, and perivascular and/or peribronchial inflammation, parenchyma injury, and hemorrhage parameters were analyzed as previously described [30]. All semiquantitative analysis was examined under a light field optical microscope for a digital image capture system (Motic 2.0).

The quantification of interalveolar septa thickening and pulmonary inflammation was performed by morphometric analysis of the 20 random images captured with a 20X magnification objective using a microscope camera (TK-1270/RGB, JVC, Japan), totaling an area of 3.2×10^6 mm^2 of analyzed parenchyma per animal. Using the KS300 software, all pixels of the lung tissue in the real image was selected for the creation of a binary image, digital processing, and calculation of the area in μm^2 of the interalveolar septum. The analysis of the pulmonary inflammatory infiltrate was performed on the images previously selected to assess the thickening of the interalveolar septum. All cells contained in each image were quantified using the Carl Zeiss Image Analyser KS300 software program. The inflammatory infiltrate in the lung was quantified by counting the number of nuclei present in the histological sections.

2.8. Macrophage N-acetylglucosaminidase and neutrophil myeloperoxidase assays

Activities of macrophage N-acetylglucosaminidase (NAG) and neutrophil myeloperoxidase (MPO) were measured in lung homogenates according to a method previously described [29]. After tissue homogenization (TissueLyser LT - Qiagen, German), the homogenate was centrifuged at 8000×*g*, 10 min at 4 °C and the remaining pellet was examined to determine the activity of NAG and MPO.

For NAG assay, the pellet was homogenized in 800 μL of NaCl 0,9 %/Triton 100 0,1 %. The lysate was then centrifuged at 300×*g*, 10 min, 4 °C and the supernatant was distributed (100 μL/well) into a 96-well microplate (Corning, USA). The reaction was started with the addition of 100 μL of the substrate *p*-nitrophenyl-N-acetyl-β-D-glucosaminide (Sigma Chemical Co., USA) diluted in citrate/phosphate buffer (0.1 M citric acid, 0.1 M Na_2 HPO_4, pH 4.5) at the final concentration of 2.24 mM and incubation at 37 °C for 10 min. The reaction was terminated by the addition of 100 μL of 0.2 M glycine buffer (0.8 M glycine, 0.8 M NaCl and NaOH, pH 10.6) and the absorbance was determined at 405 nm. The content of macrophages was calculated from a standard curve based on the expression of NAG activity made from 3 % thioglycollate stimulated peritoneal macrophages (data not shown).

For the MPO assay, the pellet was homogenized in 200 μL of buffer 1 solution (0.1 M NaCl, 0.02 M Na_3PO_4, 0.015 M Na_2EDTA, pH 4.7) followed by centrifugation at 1500×*g*, 10 min at 4 °C. 800 μL of buffer 2 solution (0.05 M NaPO4, 0.5 % hexadecyltrimethylammonium bromide) was added to the pellet and the mixture was homogenized and then frozen/thawed three times using liquid nitrogen. The lysate was centrifuged at 1500×*g*, 10 min at 4 °C and the supernatant was used for the enzymatic assay. 25 μL/well were distributed onto 96-well microplates (Corning, USA) followed by the addition of 25 μL of substrate TMB (3.3′-5.5;- tetramethylbenzine + 1.6 mM dimethylsulfoxide) and 100 μL of 0.5 M H_2O_2. After incubation for 5 min at room temperature, the reaction was stopped by the addition of 100 μL of sulphuric acid (1 M H_2SO_4). Absorbance was determined by a VersaMax ELISA microplate reader (Molecular Devices, USA) at a wavelength of 450 nm.

2.9. Measurement of cytokine profiles in lung tissues

To determine the cytokine profile of the lungs, organs were harvested and homogenized (TissueLyser LT - Qiagen, German) in extraction solution (0.4 M NaCl, 0.05 % Tween 20, 0.5 % BSA, 0.1 mM phenylmethylsulphonyl fluoride, 0.1 mM benzethonium chloride, 10 mM EDTA and 20 KI units aprotinin) at the rate of 1 mL per 100 mg of tissue. The resulting homogenates were centrifuged at 8000×*g*, 10 min at 4 °C, and the collected supernatants were stored at −80 °C. Measurements of IL-1β, IL-12/IL-23p40, IL-33 and TGF-β were measured by sandwich ELISA kit (R&D Systems, USA), according to manufacturer's instructions. The absorbance was determined by a VersaMax ELISA microplate reader (Molecular Devices, USA) at a wavelength of 492 nm, and the cytokine concentration (pg/mL) for each sample was calculated by interpolation from a standard curve. The quantification of IFN-γ, TNF-α, IL-2, IL-6, IL-4, IL-17A, and IL-10 was conducted using a cytometry bead array (CBA) (BD Bioscience, USA), according to the manufacturer's instructions. The data were collected using a FACSCalibur™ flow cytometer (BD Biosciences, USA) and the results were analyzed in FlowJo software (Tree Star, Ashland, OR).

2.10. Assessment of respiratory mechanics

The evaluation of pulmonary function was performed in infected and control mice, as previously described [30]. Briefly, after being anesthetized but still able to maintain spontaneous breathing under anesthesia, mice were tracheostomized, placed in a plethysmograph and connected to a computer-controlled ventilator (Forced Pulmonary Maneuver System® , Buxco Research Systems, Wilmington, North Carolina USA). First, an average breathing frequency of 160 breaths/min was imposed on the animal by pressure-controlled ventilation. After 3 min, the constant-phase model was used to measure dynamic compliance (Cdyn) and lung resistance (RI). A fast-flow volume maneuver was performed, and the lungs were first inflated to +30 cm H_2O and immediately afterward were connected to a highly negative pressure to force expiration until −30 cm H_2O was reached. The forced vital capacity

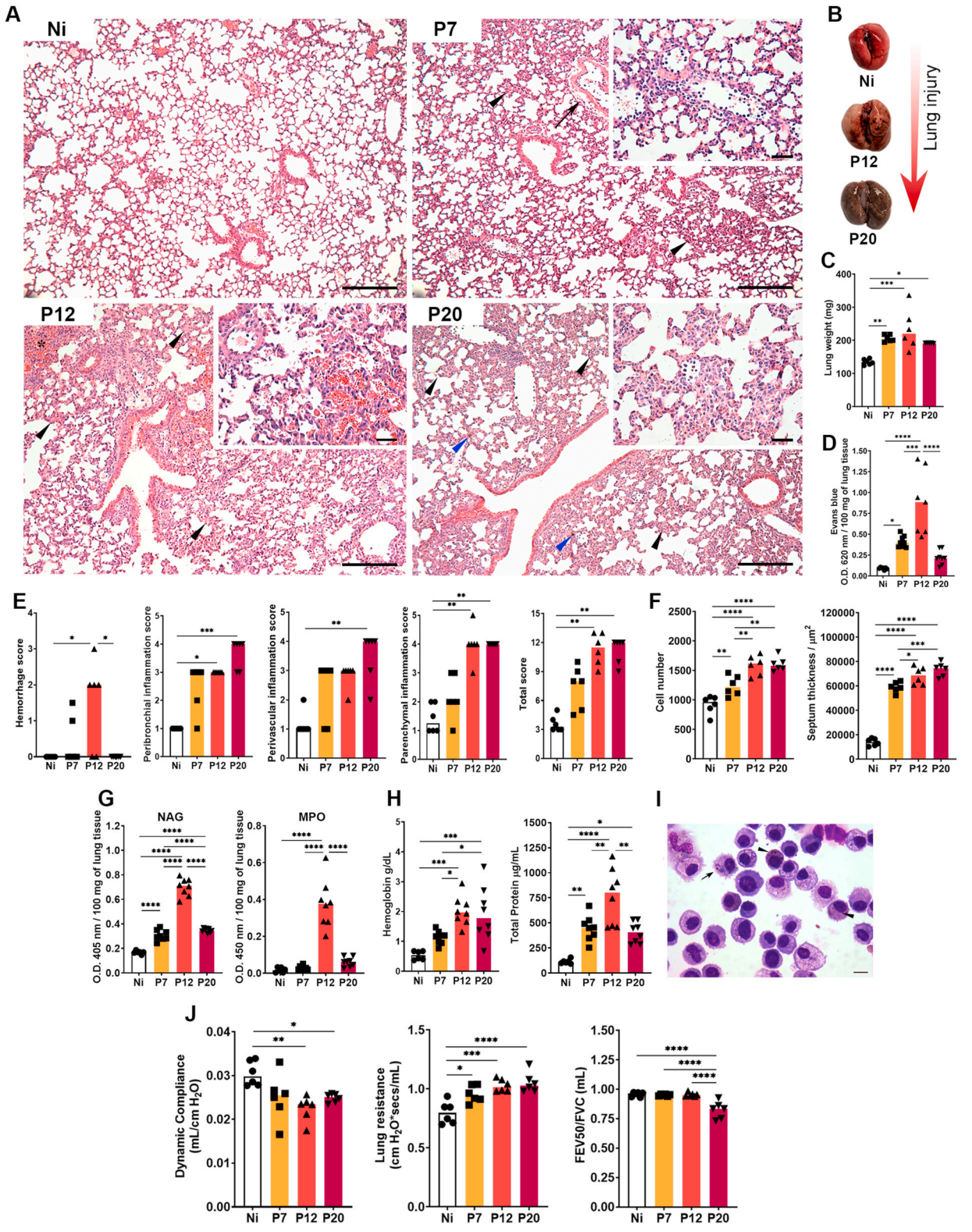

(caption on next page)

Fig. 2. Lung injury and inflammation during *P. berghei* NK65-NY infection. (A) Representative hematoxylin and eosin staining of lung sections. Interalveolar septum thickening at the expense of inflammatory infiltration (black arrowheads at 7-, 12- and 20 dpi), perivascular edema (arrow at 7 dpi). Area of hemorrhage (asterisk at 12 dpi), interstitial deposit of malarial pigment (blue arrowheads at 20 dpi). Inserts showing details of the inflammatory infiltrate (at 7-, 12- and 20 dpi). Lowest magnification scale bar = 100 μm. Scale bar of highest magnification = 10 μm. (B) Macroscopy of non-perfused lungs of *P. berghei* NK65-infected mice (Ni: non-infected control; P12: PbNK65-infected mice at 12dpi; P20: PbNK65-infected mice at 20dpi). (C) Lung weight. (D) Evans blue dye vascular permeability evaluation. (E) Lung injury and inflammation score. First graph: Hemorrhage score; second graph: Peribronchial inflammation score; third graph: Perivascular score; fourth graph: Parenchymal inflammation score; fifth graph: Total score. (F) Lung morphometry. First graph: Cellularity; second graph: Septum thickness. (G) Cellular activity. First graph: macrophage activity (NAG); second graph: neutrophils activity (MPO). (H) BAL analysis. First graph: Hemoglobin levels; second graph: Total protein levels. (I) Alveolar macrophages of *P. berghei* NK65-infected at 20 dpi phagocytize parasites (arrow) and malaria pigment inside the cells (arrowhead). (J) Pulmonary mechanics. First graph: Dynamic compliance; second graph: Lung resistance; third graph: Tiffeneau-Pinelli index. Kruskal–Wallis test followed by Dunn's test was used on score data. One-way ANOVA test followed by Tukey's multiple comparisons was used on morphometry, NAG and MPO activity and BAL data to compare the variances between the groups ($n = 6$ for control and $n = 8$ for infected mice per group). The data presented here is representative of two independent experiments. *$p < 0.05$, **$p < 0.01$, ***$p < 0.001$, and ****$p < 0.0001$. (For interpretation of the references to color in this figure legend, the reader is referred to the Web version of this article.)

(FVC) forced expiratory volume at 50 ms (FEV50) and Tiffeneau-Pinelli index (FEV50/FVC) were recorded. Each maneuver was performed three times for each parameter. Suboptimal maneuvers caused by death or insufficient anesthesia of the animal were discarded and at least three acceptable maneuvers were conducted to obtain a reliable mean for all numeric parameters.

2.11. Statistical analysis

GraphPad Prism 9.5 (GraphPad Software, Inc., USA) was used for statistical analysis. Grubb's test was used to detect sample outliers. The Shapiro–Wilk normality test was performed to assess the normality of the variables. The evaluation between three or more groups was performed using the Analysis of Variance (ANOVA) or Kruskal-Wallis test, followed by Tukey's or Dunn's post-test, respectively, according to the data distribution. Survival curves were compared using the Gehan–Breslow–Wilcoxon test. All tests were considered significant at $p \leq 0.05$.

3. Results

3.1. MA-ALI/ARDS by P. berghei NK65 infection

In this work, we investigated AMs and MO kinetics and phenotype in the BAL of C57BL/6j mice infected with 10^4 iRBCs of PbNK65-NY, euthanized at 7, 12 and 20 dpi (Fig. 1A). Firstly, we characterize pathophysiology and inflammation in the lung tissue during infection and then, describe immunophenotypes in the airways of infected animals.

In accordance with previous studies [3,30], our results showed that the parasitemia raised gradually from the 4th dpi onwards until hyperparasitemia at 24 dpi (Fig. 1B), where most of the mice succumbed to systemic damage (Fig. 1C). Sickness-related changes began to be observed from the 14th dpi, when infected animals showed a percentage of body weight loss of around 3 %, a total clinical score of 3.3, and parasitemia of around 20 %. The worsening of the clinical conditions of the infected animals occurred from the 16th dpi onwards, when the majority had reduced motility and abnormal breathing, with a percentage of body weight loss of around 10 %, an average clinical score of 7.7, and parasitemia around 40 % (Fig. 1D and E) [26,34].

Histopathological analysis of the pulmonary parenchyma allowed the observation and description of lesions caused by PbNK65 infection. In the microscopical analysis of lung parenchyma, moderate diffuse mononuclear inflammatory infiltrate, and perivascular edema were observed in infected mice at 7 dpi (Fig. 2A, upper right). These findings were even more pronounced at 12 dpi (Fig. 2A, lower left), in which moderate to intense hemorrhagic areas were also present in infected mice compared to their non-infected controls. Brownish pigment was also frequently found, suggesting deposition of hemosiderin and/or hemozoin malarial pigment (Fig. 2A, lower right, blue arrowheads). Subsequently, at 20 dpi, the inflammatory infiltrate was higher than at other times points, but hemorrhage and perivascular edema was reduced (Fig. 2A, lower right). All these injury phenomena were macroscopically observed in infected mice, where PbNK65-infected mice presented reddish areas in the lungs at 12 dpi, which were suggestive of lesions caused by the large hemorrhage area in this group (Fig. 2B), that reflects on the lung weight (Fig. 2C) and increased vascular permeability in the lung parenchyma (Fig. 2D). Corroborating with this data, semiquantitative histopathologic analysis of the lung shows a high hemorrhage score at 12 dpi and progressive increase of inflammation (Fig. 2E). These exudative events in the lung parenchyma led to increased influx of leukocytes, followed by progressive thickening of the interalveolar septa (Fig. 2F). Interestingly, NAG and MPO activity significantly increased in lung tissue at 12 dpi compared to the other groups, despite decreasing at 20 dpi (Fig. 2G). A similar profile was observed when analyzing the contents of the airways with a significant increase in hemoglobin and total protein levels in infected animals compared to the control group, especially at 12 dpi (Fig. 2H). Macrophages with parasites and malarial pigment phagocytosed in the cytoplasm were commonly found in the airways of animals infected with 12 dpi (Fig. 2I).

The large hemorrhagic areas in the lungs tissue and the high content of hemoglobin and proteins in the airways resulting from the increased pulmonary vascular permeability, added to the increased leukocyte influx over the course of the infection, may act as a contributing factor to the impairment of lung function. PbNK65-infected animals showed a decrease in dynamic compliance, and an increase in lung resistance. In addition, the infection implies a drop in the relation between the FEV50/FVC volumes at 20 dpi

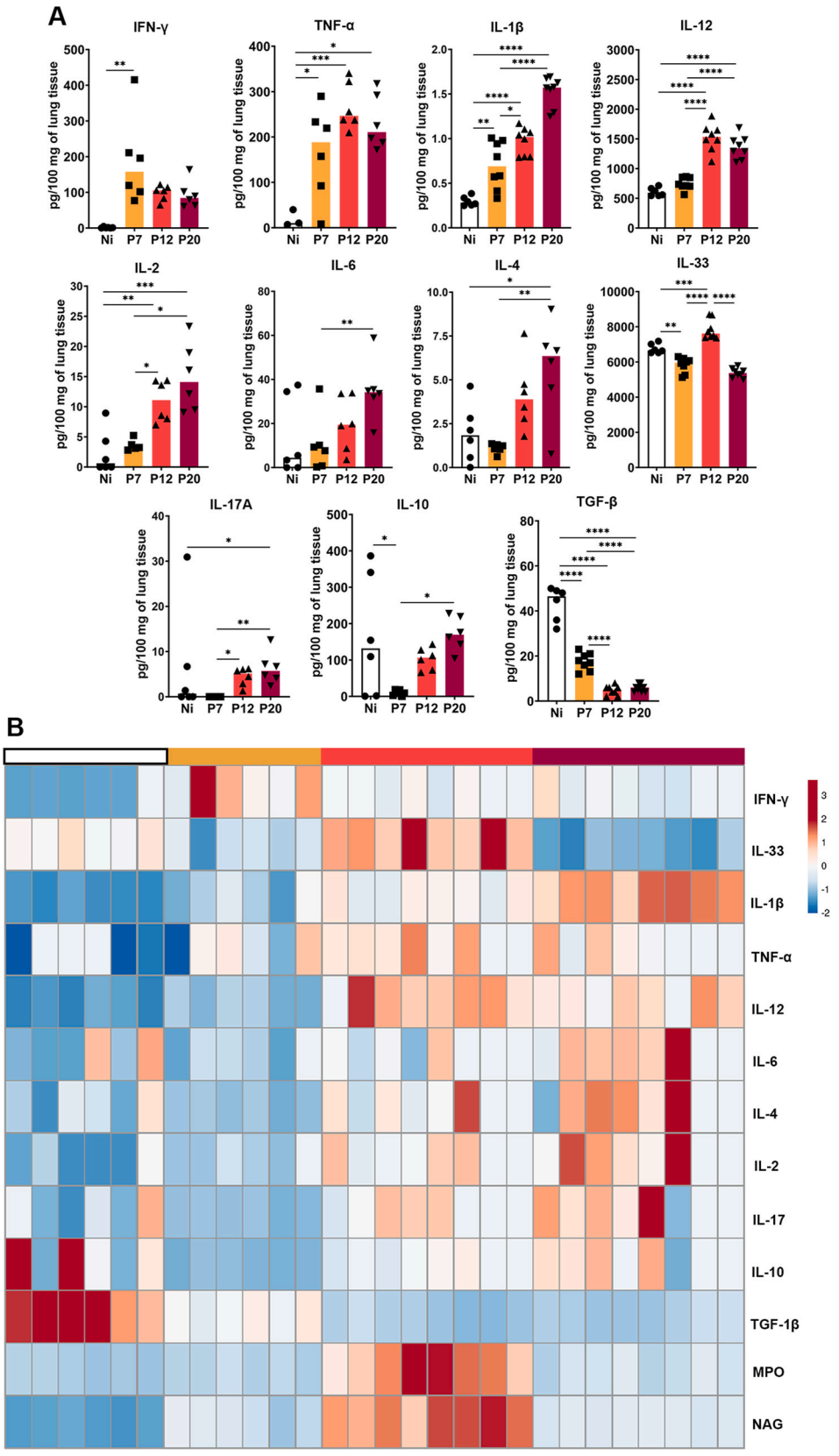

(caption on next page)

Fig. 3. Pulmonary cytokine levels induced during *P. berghei* NK65-NY infection. Supernatants of lung homogenates were used to measure the levels of cytokines by ELISA or CBA technique. (A) IFN-γ, TNF-α, IL-1β, IL-12/IL-23p40, IL-2, IL-6, IL-4, IL-17A, IL-10 and TGF-β, respectively. (B) Heatmap of the lung inflammatory profile during severe *P. berghei* NK65-NY malaria, evidencing the cytokine profile and NAG and MPO activity of lung tissue from Non-infected (Ni – white color) and PbNK65-NY-infected mice at 7 (P7 – yellow color), P12 (orange color) and P20 dpi (magenta color). n = 6 animals per group were used. Each column represents an animal, and each line represents a variable of one of the analyzed parameters. The scale presented refers to the variance values for each parameter. The Kruskal–Wallis test followed by Dunn's test was used on IL-2 and IL-6 data. One-Way ANOVA test followed by multiple comparisons test were used on the other data to compare the variances between the groups (n = 6 for control and n = 8 for infected mice, per group). The data presented here is representative of two independent experiments. *$p < 0.05$, **$p < 0.01$, ***$p < 0.001$, and ****$p < 0.0001$. (For interpretation of the references to color in this figure legend, the reader is referred to the Web version of this article.)

(Tiffeneau-Pinelli index), configuring a restrictive pathology (Fig. 4J).

3.2. Inflammatory cytokines profile in the lung tissue during PbNK65-NY infection

Regarding cytokine production in lung tissue, increased levels of cytokines IFN-γ, TNF-α and IL-1β were observed at 7 dpi. Cytokine levels remained elevated at 12 dpi, with even higher levels of TNF-α compared to other cytokines, although this trend was not sustained thereafter. However, IL-1β levels continued to increase up to 20 dpi. In contrast, IL-12/IL-23p40 and IL-2 increased only at 12 dpi and remained relatively stable until day 20, when IL-6 and IL-4 levels increased. Interestingly, only at 12 dpi was found a significant increase in IL-33 production. Increased levels of IL-17A were observed at later times, while IL-10 production showed an early reduction at 7 dpi, returning to baseline levels at 12 dpi. TGF-β was found to progressively decrease during infection, up to 12 dpi and remained low thereafter (Fig. 3A and B).

3.3. PbNK65-NY infection induces increased alveolar macrophage cellularity, CD11b$^+$ Ly6C^{low} monocytes and CD8$^+$ T cells accumulation in the airways

Subsequently, our investigation delved into characterizing cell populations in BAL (Supplementary Fig. S1) during MA-ALI/ARDS. We focused on time points 12 and 20 dpi, as alterations at 7 dpi were subtle. The decision was driven by the prominent peak in hemorrhagic score, NAG, MPO production, and proinflammatory cytokines at 12 dpi, suggesting a progression worth exploring up to 20 dpi. A significantly increased number of AMs was found at 20 dpi, and AMs populations were found to be expressing high levels of TNF-α, followed by lower expression intensity of MHC-II at 12 dpi (Fig. 4A). Furthermore, PbNK65-infected mice showed significant MOs infiltration in the airways. These MOs displayed increased expression intensity of TNF-α, MHC-II, and Ly6C at 12 dpi, however the expression of TNF-α and Ly6C was found to be slightly decreased at 20 dpi (Fig. 4B). NEUs infiltration peaking at 20 dpi with high expression intensity of TNF-α and MHC-II (Fig. 4C). CD4$^+$ T lymphocytes were recruited to the alveolar compartment peaking at 12 dpi, while CD8$^+$ T lymphocytes reached the peak at 20 dpi (Fig. 4D).

Clustering tSNE analysis was applied to further characterize the immune cell population throughout the infection. tSNE is an unbiased dimensionality reduction analysis that clusters similar cell phenotypes according to the marker's expressions. The results show three major myeloid cells populations in this model: LiveSiglec$^-$F$^+$CD11c$^+$ AM, LiveSiglec$^-$F$^-$Ly6C$^+$ MOs, and LiveSiglec$^-$F$^-$Ly6C$^-$Ly6G$^+$ NEUs, with different profiles of distribution in each group (Fig. 4E). As expected, non-infected mice showed AM as the predominant population, unlike infected animals that had, in addition to these cells, MO and NEU infiltrate. When analyzing the distribution of AM populations by tSNE-followed rPhenograph cluster identification, we found that the AMs were grouped into three different clusters: AM1, the main representative of Ni group; AM2, the majority indicative of Pb12 group and AM3, as the main representative of Pb20 group. (Fig. 4F). To characterize these populations, their expression of relevant markers was compared by representing the tSNE output as an expression heatmap. The infection led to higher expression of Siglec-F and MHC-II markers, especially at 20 dpi (Fig. 4G). The increased expression of these markers indicates the activation of AMs throughout infection. No significant differences were found regarding the distribution of MO populations in the airways according to the parameters used.

4. Discussion

MA-ALI/ARDS represents a severe manifestation of *Plasmodium* sp. infection with poor prognostic outcomes, high fatality rate, and limited therapeutic interventions [2,35]. MA-ALI/ARDS cases have been reported in infection with all human malaria parasites, although the greatest number of cases is caused by *P. falciparum* and *P. vivax* [36–38]. Given the challenges in studying malaria in humans, the use of experimental models has facilitated the comprehension of MA-ALI/ARDS. As a result, animal models of MA-ALI/ARDS play a crucial role in conducting mechanistic investigations, identifying potential interventions, and validating hypotheses derived from clinical studies [39–41]. Here, we used the severe malaria experimental model of C57BL/6j mice infected with PbNK65-NY to understand the pathophysiology associated with the dynamics of AMs and infiltrating leukocytes subpopulations in the airways in pulmonary malaria. As expected, our results show that PbNK65-infected animals had high morbidity and mortality with increasing parasitemia. MA-ALI/ARDS is usually associated with increased vascular permeability, edema, hemorrhage and inflammation in the lungs, characteristics found in our model [2,30].

Alveolar macrophages (AM) play a crucial role in host defense, tissue homeostasis, pathogen recognition, initiation and resolution of lung inflammation, and repair of damaged tissue. Under homeostatic conditions, AMs play a pivotal role in maintaining lung physiology, particularly in the uptake and regulation of surfactant within the alveoli [13]. Perturbations in the surfactant composition

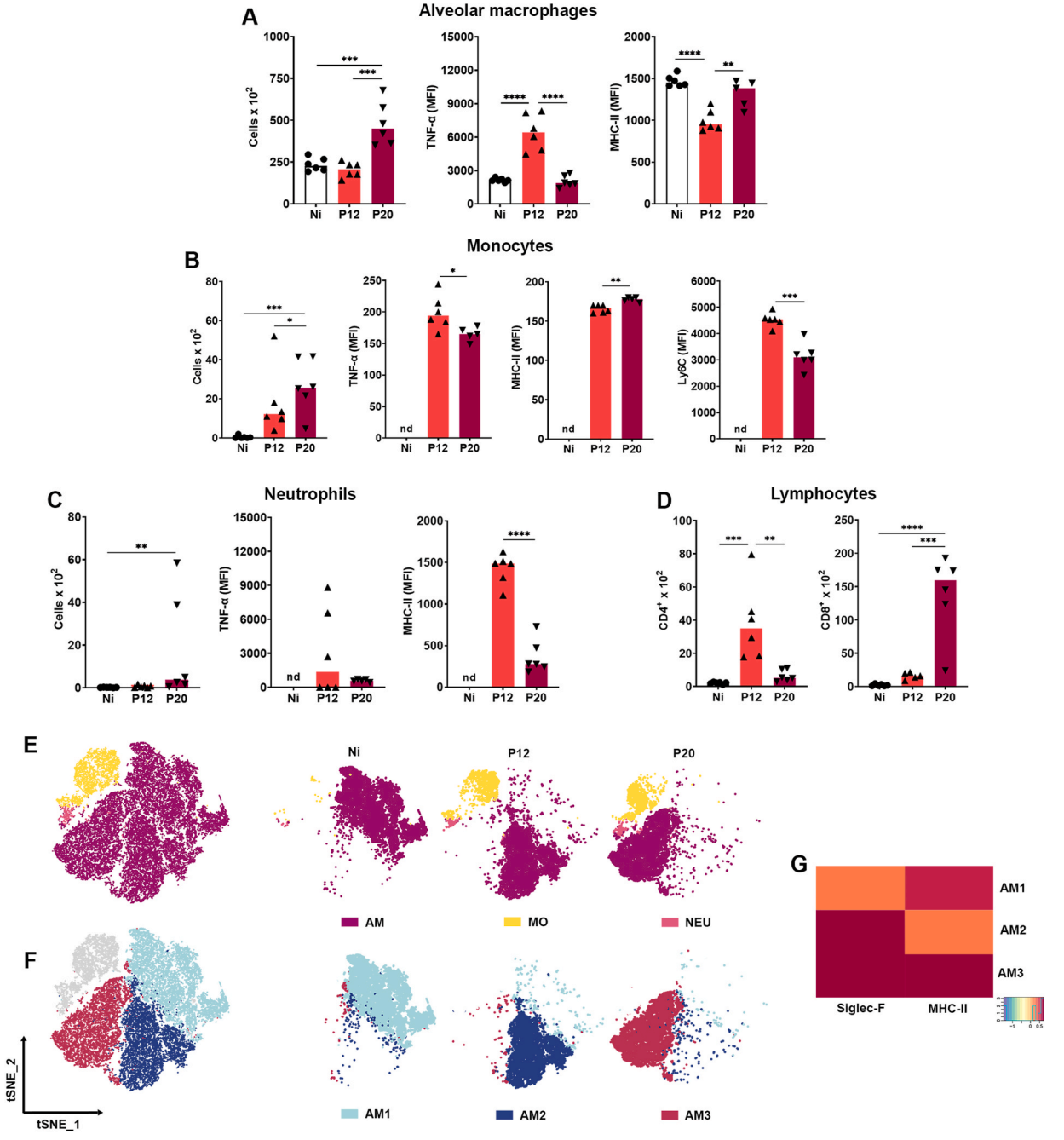

(caption on next page)

Fig. 4. Flow cytometry analysis of myeloid and lymphoid BAL cells during *P. berghei* NK65-NY infection. (A) Alveolar macrophages. First graph: Total alveolar macrophages count; second graph: Frequency of TNF-α in alveolar macrophages; third graph: mean intensity of fluorescence (MFI) of MHC-II in alveolar macrophages. (B) Monocytes. First graph: Total monocytes count; second graph: MFI of TNF- α in monocytes; third graph: MFI of MHC-II in monocytes; fourth graph: MFI of LY6C in monocytes. (C) Neutrophils. First graph: Total neutrophil count; second graph: MFI of TNF- α in neutrophil; third graph: MFI of MHC-II in neutrophils. (D) Lymphocytes. First graph: Total $CD4^+$ T lymphocyte count; second graph: Total $CD8^+$ T lymphocyte count. (E) Unbiased high dimensional analysis of flow cytometry data (tSNE) of BAL cells: Alveolar macrophages "AM", monocytes "MO", and neutrophils "NEU". (F) Unbiased high dimensional analysis of flow cytometry data (tSNE) of BAL. AM cells for all groups, indicating 3 a. m. subpopulations based on the expression of surface markers, each cluster indicated by a number and color. (G) Heatmap evidencing the expression level of surface markers (Siglec-F and MHC-II) within each AM subpolulations. Kruskal–Wallis test followed by Dunn's test was used on MFI of TNF-α, in MOs, and neutrophils data. One-way ANOVA test followed by Tukey's multiple comparisons was used on alveolar macrophages, and lymphocytes, to compare the variances between the groups ($n = 6$ for control and $n = 8$ for infected mice, per group). An average of 5.2×10^4 events was acquired for BAL flow cytometry analyses. The data presented here is representative of two independent experiments. *$p < 0.05$, **$p < 0.01$, ***$p < 0.001$, and ****$p < 0.0001$. Cell clusters and the signature scores are indicated at the x- and y-axis, respectively. (For interpretation of the references to color in this figure legend, the reader is referred to the Web version of this article.)

can lead to respiratory distress, as observed in ALI/ARDS [42,43]. Studies have demonstrated increased expression levels of surfactant protein-D (SP-D) and altered profile of lipids in lung tissues and elevated plasma SP-D levels in malaria-infected mice with MA-ALI/ARDS [44,45]. These findings suggest a potential link between AMs dysfunction, surfactant regulation, and the pathogenesis of ALI/ARDS in the context of malaria infection. Nevertheless, the role of AMs in MA-ALI/ARDS remains insufficiently understood [24,25,46,47].

Acute inflammation or severe infections can result in the loss of AMs population [19–21]. In order to preserve lung function and respiratory exchange caused by these insults, the alveolar niche can be recomposed through self-renewal of the remaining AMs, or through partial or total occupancy of recruited MOs that later differentiate into MO-DCs or MO-Macs similar to AMs [48–50]. It has been reported that AMs can be at least partially depleted in inflammatory processes such as influenza infection [19], pneumonitis [20], COVID-19 [21], and pulmonary fibrosis [22]. In malaria, some studies have shown that lung-resident macrophage populations may not change during experimental *P. berghei* ANKA infection [23–25]. On the other hand, Lai and colleagues show that AMs depletion is related to malaria infection, but that these cells self-renew after resolution without the need for replacement via circulating MOs on non-lethal *P. yoelii* infection [46]. Interestingly, we found a delayed increase in the number of AMs in the airways of PbNK65-infected animals. The proliferation of AMs was demonstrated by Oliveira et al. (2022) in an LPS-induced ARDS model in $CCR2^{-/-}$ mice [51]. The authors showed that the recovery of the niche of these cells occurs through self-renewal in the absence of the receptor, indicating that the migration of $CCR2^+$ MOs from the marrow does not interfere with the development of the disease [51].

Constitutively, AMs express high levels of CD11c and Siglec-F, which allows the separation of long-lived AMs (cells that have adapted to the local microenvironment) and transient MO-derived cells that have been recruited into the alveolar space during inflammation [13,52].In this work, we show that AMs populations can vary during infection based on different levels of Siglec-F and MHC-II expression, although the role of Siglec-F in AMs is not clear [53,54], we suggest that the modulation of this marker is involved in the activation state alterations of AMs during PbNK65 infection [55,56]. This modulation of AM populations may be a reflection of disruption of the blood-alveolar barrier. In our model, we observed an increase in exudative phenomena mainly at 12 dpil. This process involves the production of chemokines, such as CCL2, CCL5, CXCL10, CXCL8, which promote the influx of leukocytes into the alveolar environment. While iRBC are not typically found within the pulmonary alveoli, it is noteworthy that certain immune cells can become activated in the lung tissue and subsequently migrate to the alveolar space. Our research has focused on precisely this phenomenon, examining the cellular composition of the bronchoalveolar space. Our findings revealed the presence of MOs, NEUs, $CD4^+$ and $CD8^+$ lymphocytes, within this compartment. The presence of NEUs expressing MHC-II, found in our study, is important to highlight how acute infections can induce phenotype changes in immune cells. NEUs were shown to start expressing antigen-presenting molecules (specifically MHC-II) and costimulatory molecules, in the context of infection with high levels of inflammatory cytokines. Previous studies have shown that NEUs can be converted into antigen-presenting cells, after acquiring dendritic cells (DCs) surface markers such as $CD11c^+$ $MHCII^+$, in addition to the expression of the costimulatory molecules CD80 and CD86 [57]. Recently, NEUs were found to be expressing MHC II molecules during bovine mastitis caused by bacterial infection [58]. It was also shown the role of NEUs in phagocytosis of erythrocytes, and subsequently, NEUs start expressing MHC-II, CD40 and CD80, displaying ability to elicit antigen-specific T cell response [59]. These findings highlight the plasticity ability of immune cells to respond against foreign stimuli. In our case, considering that malaria is an infection with powerful inflammatory stimulation, it can contribute to changes in NEUs phenotype leading to increased MHC-II expression and, possibly, to develop antigen-presenting characteristics. Notably, these infiltrating immune cells possess the capacity to further stimulate AMs, thereby modulating their functional state. This interplay between immune cells in the bronchoalveolar space and AMs highlights the intricate orchestration of immune responses within the pulmonary microenvironment.

MOs play an important role in homeostasis and innate and adaptive immunity during inflammatory processes but can also contribute to several pathologies [60–63]. The involvement of $Ly6C^+$ MOs subpopulations has been discussed in various infections, such as *Toxoplasma gondii* [64–66], *Leishmania major* [67,68], and *Schistosoma mansoni* [69,70]. Nevertheless, the dynamics of these MOs subpopulations in malaria remain a subject of ongoing debate and lack of consensus [71]. Consistent with previous findings [24,72], our data reveal an accumulation of $Ly6C^{low}$ MOs in the lungs. However, in our model, this accumulation occurred at a later stage in the airways. In contrast, Lai et al. demonstrated a distinct pattern in the *P. yoelii* infection model, where the prevalence of $Ly6C^{hi}$ MOs in the lungs persisted throughout the infection [46]. On the other hand, studies have demonstrated that experimental PbANKA

infection, does not alter AM populations, despite the increased accumulation of Ly6C^{high} MOs in the lungs [23–25]. Nevertheless, Pollenus et al. show that Ly6C^{high} inflammatory MOs accumulate in the lungs after infection and remain increased even after treatment with antimalarial drugs, in which the number of non-classical Ly6C^{low} MOs and DCs is increased. These results may explain the dynamics of accumulation in transient MOs Ly6C^{high} to Ly6C^{low} also found in our model, since Ly6C^{low} MO plays a role in tissue remodeling and, as well as Ly6C^{high} MOs, can differentiate into monocyte-derived dendritic cells (MO-DC) capable of performing antigen presentation [25].

CD8$^+$ T cells play a crucial role in the pathogenesis of MA-ARDS both in experimental models and in humans [3,7,9,73]. Although our results showed a delayed accumulation of CD4$^+$ and CD8$^+$ lymphocytes in relation to the findings from other groups [25,74], it is important to emphasize that differences between each infection model (species, strain, inoculum, host), target study environment (lung, airways) can interfere with the outcome and dynamics of the infection pathology. In this sense, the previous absence of infiltrated leukocytes in the alveolar space does not necessarily exclude the possibility of these cells' presence in the tissue and vice versa [39,41,75,76].

Nevertheless, we show that PbNK65 infection induces a lethal course, marked by hemorrhagic events and intense inflammation, mediated by increased levels of IFN-γ, TNF-α, IL-1β, IL-12, IL-2 and IL-33, and downregulation of TGF-β and IL-10. This polarized inflammation supports a sepsis-like process marked by the general deterioration of the health of infected mice throughout the course of infection, as observed in some human cases of *P. vivax* and *P. falciparum* malaria [77–85]. Interestingly, we found increased levels of the cytokine IL-33 only at 12 dpi. In fact, some studies have shown that elevated levels of IL-33 and MPO are associated with worsening inflammation in LPS-induced ALI [86], IL-1β production in gouty arthritis [87], in addition to stimulating the formation of neutrophil extracellular traps (NETs), oxidative stress and the secretion of proatherogenic factors in advanced atherosclerosis [88]. Despite all these phenomena at 12 dpi, animal mortality was observed only after 20 dpi, when pulmonary hemorrhage and NAG and MPO activity decreased. This inflammatory environment could be a contributing factor to the breakdown of the blood-alveolar barrier, which resulted in an increase the population and activation phenotype of the AMs, as well as the accumulation of Ly6C^{low} MOs, NEUs and CD4$^+$ and CD8$^+$ lymphocytes in the airways.

However, it is important to note that, despite the absence of apparent hemorrhage and the decrease in NAG and MPO activity on day 20, the constant inflammation caused by the presence of the parasite was a decisive factor for the worsening of the disease, which could be detrimental to the respiratory function and, consequently, the mortality of the animals. It is important to note that NAG and MPO activity, and the cytokines levels were measured in the lung tissue and not in the bronchoalveolar lavage. These represent two distinct compartments, and this limitation should be considered when interpreting the results in our study. Taken together, our study provides new insights into the alveoli pathophysiology of MA-ALI/ARDS, highlighting potential targets for therapeutic interventions.

Funding

This research was financially supported by Fundação de Amparo à Pesquisa do Estado de Minas Gerais/FAPEMIG, Brazil (Grant #APQ-4035/17), Rede Mineira de Imunobiológicos (RED-00067-23), and Conselho Nacional de Desenvolvimento Científico e Tecnológico (CNPq) Demanda Universal (Grant # 403278/2023-6). RTF (Grant #305514/2022-9) and LLB (#310311/2023-3) are research fellows of the CNPq. FVS is recipient of PhD Scholarship from the Minas Gerais State Agency for Research and Development (FAPEMIG). LMDM and RMMB are recipients of post-doctoral fellowships from Coordenação de Aperfeiçoamento de Pessoal de Nível Superior (CAPES) and FAPEMIG, respectively.

Data availability statement

The original contributions presented in the study are included in the article/supplementary material. Further inquiries can be directed to the corresponding author.

CRediT authorship contribution statement

Flaviane Vieira-Santos: Writing – original draft, Methodology, Investigation, Formal analysis, Data curation, Conceptualization. **Ramayana Morais de Medeiros Brito:** Methodology, Investigation, Formal analysis, Data curation, Writing – original draft, Writing – review & editing. **Camila de Almeida Lopes:** Methodology, Investigation, Formal analysis, Data curation. **Thais Leal-Silva:** Methodology, Investigation, Data curation. **Jorge Lucas Nascimento Souza:** Methodology, Investigation, Formal analysis. **Chiara Cássia Oliveira Amorim:** Methodology, Investigation, Formal analysis. **Ana Cristina Loiola Ruas:** Methodology, Investigation, Formal analysis. **Luiza de Lima Silva Padrão:** Methodology, Investigation, Formal analysis. **Lucas Kraemer:** Supervision, Investigation, Formal analysis. **Fabrício Marcus Silva Oliveira:** Methodology, Investigation, Formal analysis. **Marcelo Vidigal Caliari:** Visualization, Methodology, Investigation, Formal analysis. **Remo Castro Russo:** Writing – review & editing, Resources, Methodology, Investigation, Formal analysis, Data curation. **Ricardo Toshio Fujiwara:** Writing – review & editing, Visualization, Resources, Investigation, Funding acquisition, Conceptualization. **Luisa Mourão Dias Magalhães:** Writing – review & editing, Visualization, Supervision, Methodology, Investigation, Formal analysis, Conceptualization. **Lilian Lacerda Bueno:** Writing – review & editing, Visualization, Supervision, Resources, Project administration, Methodology, Investigation, Funding acquisition, Conceptualization.

Declaration of competing interest

The authors declare that they have no known competing financial interests or personal relationships that could have appeared to influence the work reported in this paper.

Acknowledgments

We would like to thank Michele Silva de Matos and Vanessa Gomes Fraga for their technical assistance and support during the experiments. Figures were made using biorender.com.

Appendix A. Supplementary data

Supplementary data to this article can be found online at https://doi.org/10.1016/j.heliyon.2024.e33739.

References

[1] WHO, World malaria report 2022. https://www.who.int/teams/global-malaria-programme/reports/world-malaria-report-2021, 2022.
[2] P.E. Van den Steen, K. Deroost, J. Deckers, E. Van Herck, S. Struyf, G. Opdenakker, Pathogenesis of malaria-associated acute respiratory distress syndrome, Trends Parasitol. 29 (2013) 346–358, https://doi.org/10.1016/j.pt.2013.04.006.
[3] P.E. Van Den Steen, N. Geurts, K. Deroost, I. Van Aelst, S. Verhenne, H. Heremans, J. Van Damme, G. Opdenakker, Immunopathology and dexamethasone therapy in a new model for malaria-associated acute respiratory distress syndrome, Am. J. Respir. Crit. Care Med. 181 (2010) 957–968, https://doi.org/10.1164/rccm.200905-0786OC.
[4] S. Epiphanio, M.G. Campos, A. Pamplona, D. Carapau, A.C. Pena, R. Ataíde, C.A.A. Monteiro, N. Félix, A. Costa-Silva, C.R.F. Marinho, S. Dias, M.M. Mota, VEGF promotes malaria-associated acute lung injury in Mice, PLoS Pathog. 6 (2010) 1–10, https://doi.org/10.1371/journal.ppat.1000916.
[5] K. Deroost, A. Tyberghein, N. Lays, S. Noppen, E. Schwarzer, E. Vanstreels, M. Komuta, M. Prato, J.W. Lin, A. Pamplona, C.J. Janse, P. Arese, T. Roskams, D. Daelemans, G. Opdenakker, P.E. Van Den Steen, Hemozoin induces lung inflammation and correlates with malaria-associated acute respiratory distress syndrome, Am. J. Respir. Cell Mol. Biol. 48 (2013) 589–600, https://doi.org/10.1165/rcmb.2012-0450OC.
[6] R.T. Gazzinelli, P. Kalantari, K.A. Fitzgerald, D.T. Golenbock, Innate sensing of malaria parasites, Nat. Rev. Immunol. 14 (2014) 744–757, https://doi.org/10.1038/nri3742.
[7] T.T. Pham, M. Verheijen, L. Vandermosten, K. Deroost, S. Knoops, K. Van den Eynde, L. Boon, C.J. Janse, G. Opdenakker, P.E. Van den Steen, Pathogenic CD8+ T cells cause increased levels of VEGF-A in experimental malaria-associated acute respiratory distress Syndrome, but therapeutic VEGFR inhibition Is not effective, Front. Cell. Infect. Microbiol. 7 (2017) 1–10, https://doi.org/10.3389/fcimb.2017.00416.
[8] F. Val, K. Machado, L. Barbosa, J.L. Salinas, A.M. Siqueira, M.G. Costa-Alecrim, et al., Respiratory Complications of Plasmodium vivax malaria, Am J Trop Med Hyg 97 (2017) 733–743, https://doi.org/10.4269/ajtmh.17-0131.
[9] C. Claser, S.Y.T. Nguee, A. Balachander, S. Wu Howland, E. Becht, B. Gunasegaran, S.V. Hartimath, A.W.Q. Lee, J. Theng Theng Ho, C. Bing Ong, E.W. Newell, J. Goggi, L. Guan Ng, L. Renia, Lung endothelial cell antigen cross-presentation to CD8+T cells drives malaria-associated lung injury, Nat. Commun. 10 (2019) 1–16, https://doi.org/10.1038/s41467-019-12017-8.
[10] E.B. Belachew, Immune response and evasion mechanisms of plasmodium falciparum parasites, J. Immunol. Res. 2018 (2018), https://doi.org/10.1155/2018/6529681.
[11] R. Kumar, J.R. Loughland, S.S. Ng, M.J. Boyle, C.R. Engwerda, The regulation of CD4+ T cells during malaria, Immunol. Rev. 293 (2020) 70–87, https://doi.org/10.1111/imr.12804.
[12] S.P. Kurup, N.S. Butler, J.T. Harty, T cell-mediated immunity to malaria, Nat. Rev. Immunol. 19 (2019) 457–471, https://doi.org/10.1038/s41577-019-0158-z.
[13] N. Joshi, J.M. Walter, A.V. Misharin, Alveolar macrophages, Cell. Immunol. 330 (2018) 86–90, https://doi.org/10.1016/j.cellimm.2018.01.005.
[14] A. Kelly, C. McCarthy, Pulmonary alveolar proteinosis syndrome, Semin. Respir. Crit. Care Med. 41 (2020) 288–298, https://doi.org/10.1055/s-0039-3402727.
[15] P. Cheng, S. Li, H. Chen, Macrophages in lung injury, repair and fibrosis, Cells 10 (2021) 1–17, https://doi.org/10.3390/cells10020436.
[16] T. Lazarov, S. Juarez-Carreño, N. Cox, F. Geissmann, Physiology and diseases of tissue-resident macrophages, Nature 618 (2023) 698–707, https://doi.org/10.1038/s41586-023-06002-x.
[17] H. Aegerter, B.N. Lambrecht, C.V. Jakubzick, Biology of lung macrophages in health and disease, Immunity 55 (2022) 1564–1580, https://doi.org/10.1016/j.immuni.2022.08.010.
[18] B. Allard, A. Panariti, J.G. Martin, Alveolar macrophages in the resolution of inflammation, tissue repair, and tolerance to infection, Front. Immunol. 9 (2018) 1–7, https://doi.org/10.3389/fimmu.2018.01777.
[19] C. Schneider, S.P. Nobs, A.K. Heer, M. Kurrer, G. Klinke, N. van Rooijen, J. Vogel, M. Kopf, Alveolar macrophages are essential for protection from respiratory failure and associated morbidity following influenza virus infection, PLoS Pathog. 10 (2014), https://doi.org/10.1371/journal.ppat.1004053.
[20] A. Franken, P. Van Mol, S. Vanmassenhove, E. Donders, R. Schepers, T. Van Brussel, C. Dooms, J. Yserbyt, N. De Crem, D. Testelmans, W. De Wever, K. Nackaerts, J. Vansteenkiste, R. Vos, S. Humblet-Baron, D. Lambrechts, E. Wauters, Single-cell transcriptomics identifies pathogenic T-helper 17.1 cells and pro-inflammatory monocytes in immune checkpoint inhibitor-related pneumonitis, J. Immunother. Cancer 10 (2022), https://doi.org/10.1136/jitc-2022-005323.
[21] E. Wauters, P. Van Mol, A.D. Garg, S. Jansen, Y. Van Herck, L. Vanderbeke, A. Bassez, B. Boeckx, B. Malengier-Devlies, A. Timmerman, T. Van Brussel, T. Van Buyten, R. Schepers, E. Heylen, D. Dauwe, C. Dooms, J. Gunst, G. Hermans, P. Meersseman, D. Testelmans, J. Yserbyt, S. Tejpar, W. De Wever, P. Matthys, M. Bosisio, M. Casaer, F. De Smet, P. De Munter, S. Humblet-Baron, A. Liston, N. Lorent, K. Martinod, P. Proost, J. Raes, K. Thevissen, R. Vos, B. Weynand, C. Wouters, J. Neyts, J. Wauters, J. Qian, D. Lambrechts, Discriminating mild from critical COVID-19 by innate and adaptive immune single-cell profiling of bronchoalveolar lavages, Cell Res. 31 (2021) 272–290, https://doi.org/10.1038/s41422-020-00455-9.
[22] T. Shi, L. Denney, H. An, L.P. Ho, Y. Zheng, Alveolar and lung interstitial macrophages: definitions, functions, and roles in lung fibrosis, J. Leukoc. Biol. 110 (2021) 107–114, https://doi.org/10.1002/JLB.3RU0720-418R.
[23] H.A.D. Lagassé, I.U. Anidi, J.M. Craig, N. Limjunyawong, A.K. Poupore, W. Mitzner, A.L. Scott, Recruited monocytes modulate malaria-induced lung injury through CD36-mediated clearance of sequestered infected erythrocytes, J. Leukoc. Biol. 99 (2016) 659–671, https://doi.org/10.1189/jlb.4hi0315-130rrr.
[24] P. Niewold, A. Cohen, C. van Vreden, D.R. Getts, G.E. Grau, N.J.C. King, Experimental severe malaria is resolved by targeting newly-identified monocyte subsets using immune-modifying particles combined with artesunate, Commun. Biol. 1 (2018), https://doi.org/10.1038/s42003-018-0216-2.
[25] E. Pollenus, T.T. Pham, L. Vandermosten, H. Possemiers, S. Knoops, G. Opdenakker, P.E. Van den Steen, CCR2 is dispensable for disease resolution but required for the restoration of leukocyte homeostasis upon experimental malaria-associated acute respiratory distress syndrome, Front. Immunol. 11 (2021) 1–17, https://doi.org/10.3389/fimmu.2020.628643.

[26] L. Vandermosten, C. De Geest, S. Knoops, G. Thijs, K.E. Chapman, K. De Bosscher, G. Opdenakker, P.E. Van Den Steen, 11B-Hydroxysteroid dehydrogenase type 1 has No effect on survival during experimental malaria but affects parasitemia in a parasite strain-specific manner, Sci. Rep. 7 (2017) 1–11, https://doi.org/10.1038/s41598-017-14288-x.

[27] L. Belayev, R. Busto, W. Zhao, M.D. Ginsberg, Quantitative evaluation of blood-brain barrier permeability following middle cerebral artery occlusion in rats, Brain Res. 739 (1996) 88–96, https://doi.org/10.1016/S0006-8993(96)00815-3.

[28] J. Moitra, S. Sammani, J.G.N. Garcia, Re-evaluation of Evans Blue dye as a marker of albumin clearance in murine models of acute lung injury, Transl. Res. 150 (2007) 253–265, https://doi.org/10.1016/j.trsl.2007.03.013.

[29] T. Leal-Silva, C. de A. Lopes, F. Vieira-Santos, F.M.S. Oliveira, L. Kraemer, L. de L.S. Padrão, C.C.O. Amorim, J.L.N. Souza, R.C. Russo, R.T. Fujiwara, L.M. D. Magalhães, L.L. Bueno, IL-17RA receptor signaling contributes to lung inflammation and parasite burden during Toxocara canis infection in mice, Front. Immunol. 13 (2022) 1–18, https://doi.org/10.3389/fimmu.2022.864632.

[30] F. Vieira-Santos, T. Leal-Silva, L. de Lima Silva Padrão, A.C.L. Ruas, D.S. Nogueira, L. Kraemer, F.M.S. Oliveira, M.V. Caliari, R.C. Russo, R.T. Fujiwara, L. L. Bueno, Concomitant experimental coinfection by Plasmodium berghei NK65-NY and Ascaris suum downregulates the Ascaris-specific immune response and potentiates Ascaris-associated lung pathology, Malar. J. 20 (2021) 1–15, https://doi.org/10.1186/s12936-021-03824-w.

[31] H. Chen, M.C. Lau, M.T. Wong, E.W. Newell, M. Poidinger, J. Chen, Cytofkit: a bioconductor package for an integrated mass cytometry data analysis pipeline, PLoS Comput. Biol. 12 (2016) 1–17, https://doi.org/10.1371/journal.pcbi.1005112.

[32] T. Metsalu, J. Vilo, ClustVis: a web tool for visualizing clustering of multivariate data using Principal Component Analysis and heatmap, Nucleic Acids Res 43 (2015) W566–70, https://doi.org/10.1093/nar/gkv468.

[33] J.C. Horvat, K.W. Beagley, M.A. Wade, J.A. Preston, N.G. Hansbro, D.K. Hickey, G.E. Kaiko, P.G. Gibson, P.S. Foster, P.M. Hansbro, Neonatal chlamydial infection induces mixed T-cell responses that drive allergic airway disease, Am. J. Respir. Crit. Care Med. 176 (2007) 556–564, https://doi.org/10.1164/rccm.200607-1005OC.

[34] R.W. Carroll, M.S. Wainwright, K.Y. Kim, T. Kidambi, N.D. Gómez, T. Taylor, K. Haldar, A rapid murine coma and behavior scale for quantitative assessment of murine cerebral malaria, PLoS One 5 (2010) 1–12, https://doi.org/10.1371/journal.pone.0013124.

[35] W.R.J. Taylor, J. Hanson, G.D.H. Turner, N.J. White, A.M. Dondorp, Respiratory manifestations of malaria, Chest 142 (2012) 492–505, https://doi.org/10.1378/chest.11-2655.

[36] F. Val, K. Machado, L. Barbosa, J.L. Salinas, A.M. Siqueira, M.G.C. Alecrim, H. Del Portillo, Q. Bassat, W.M. Monteiro, M.V.G. Lacerda, Respiratory complications of plasmodium vivax malaria: systematic review and meta-analysis, Am. J. Trop. Med. Hyg. 97 (2017) 733–743, https://doi.org/10.4269/ajtmh.17-0131.

[37] C.A. Moxon, M.P. Gibbins, D. McGuinness, D.A. Milner, M. Marti, New insights into malaria pathogenesis, Annu. Rev. Pathol. Mech. Dis. 15 (2020) 315–343, https://doi.org/10.1146/annurev-pathmechdis-012419-032640.

[38] A.P. Phyo, P. Dahal, M. Mayxay, E.A. Ashley, Clinical impact of vivax malaria: a collection review, PLoS Med. 19 (2022) 1–23, https://doi.org/10.1371/journal.pmed.1003890.

[39] A.G. Craig, G.E. Grau, C. Janse, J.W. Kazura, D. Milner, J.W. Barnwell, G. Turner, J. Langhorne, The role of animal models for research on severe malaria, PLoS Pathog. 8 (2012), https://doi.org/10.1371/journal.ppat.1002401.

[40] S.Y.T. Nguee, J.W.B.D. Júnior, S. Epiphanio, L. Rénia, C. Claser, Experimental models to study the pathogenesis of malaria-associated acute respiratory distress syndrome, Front. Cell. Infect. Microbiol. 12 (2022) 1–23, https://doi.org/10.3389/fcimb.2022.899581.

[41] A.C. Olatunde, D.H. Cornwall, M. Roedel, T.J. Lamb, Mouse models for unravelling immunology of blood stage malaria, Vaccines 10 (2022), https://doi.org/10.3390/vaccines10091525.

[42] W.Y. Kim, S.B. Hong, Sepsis and acute respiratory distress syndrome: recent update, Tuberc. Respir. Dis. 79 (2016) 53–57, https://doi.org/10.4046/trd.2016.79.2.53.

[43] C.W. Agudelo, G. Samaha, I. Garcia-Arcos, Alveolar lipids in pulmonary disease. A review, Lipids Health Dis. 19 (2020) 1–21, https://doi.org/10.1186/s12944-020-01278-8.

[44] D. Scaccabarozzi, K. Deroost, N. Lays, F.O. Salè, P.E. Van Den Steen, D. Taramelli, Altered lipid composition of surfactant and lung tissue in murine experimental malaria-associated acute respiratory distress syndrome, PLoS One 10 (2015) 1–16, https://doi.org/10.1371/journal.pone.0143195.

[45] C. Punsawad, P. Viriyavejakul, Expression of sphingosine kinase 1 and sphingosine 1-phosphate receptor 3 in malaria-associated acute lung injury/acute respiratory distress syndrome in a mouse model, PLoS One 14 (2019) 1–17, https://doi.org/10.1371/journal.pone.0222098.

[46] S.M. Lai, J. Sheng, P. Gupta, L. Renia, K. Duan, F. Zolezzi, K. Karjalainen, E.W. Newell, C. Ruedl, Organ-specific fate, recruitment, and refilling dynamics of tissue-resident macrophages during blood-stage malaria, Cell Rep. 25 (2018) 3099–3109.e3, https://doi.org/10.1016/j.celrep.2018.11.059.

[47] P. Gupta, S.M. Lai, J. Sheng, P. Tetlak, A. Balachander, C. Claser, L. Renia, K. Karjalainen, C. Ruedl, Tissue-resident CD169+ macrophages form a crucial front line against plasmodium infection, Cell Rep. 16 (2016) 1749–1761, https://doi.org/10.1016/j.celrep.2016.07.010.

[48] AB Khan, CS Robbins, Macrophage niche availability enables local monocyte proliferation in peripheral tissues, Nat Immunol 24 (2023) 743–745, https://doi.org/10.1038/s41590-023-01482-5.

[49] FP Martin, C Jacqueline, J Poschmann, A Roquilly, Alveolar Macrophages: Adaptation to Their Anatomic Niche during and after Inflammation, Cells 10 (2020) 2720, https://doi.org/10.3390/cells10102720.

[50] A Rigamonti, J Villar, E Segura, Monocyte differentiation within tissues: a renewed outlook, Trends Immunol 44 (2023) 999–1013, https://doi.org/10.1016/j.it.2023.10.005.

[51] VLS Oliveira, E Pollenus, N Berghmans, CM Queiroz-Junior, M Blanter, MS Mattos, et al., Absence of CCR2 Promotes Proliferation of Alveolar Macrophages That Control Lung Inflammation in Acute Respiratory Distress Syndrome in Mice, Int J Mol Sci 23 (2022) 12920, https://doi.org/10.3390/ijms232112920.

[52] A.V. Misharin, L. Morales-Nebreda, G.M. Mutlu, G.R.S. Budinger, H. Perlman, Flow cytometric analysis of macrophages and dendritic cell subsets in the mouse lung, Am. J. Respir. Cell Mol. Biol. 49 (2013) 503–510, https://doi.org/10.1165/rcmb.2013-0086MA.

[53] Y.H. Feng, H. Mao, Expression and preliminary functional analysis of Siglec-F on mouse macrophages, J. Zhejiang Univ. - Sci. B. 13 (2012) 386–394, https://doi.org/10.1631/jzus.B1100218.

[54] A.L. McCubbrey, L. Barthel, M.P. Mohning, E.F. Redente, K.J. Mould, S.M. Thomas, S.M. Leach, T. Danhorn, S.L. Gibbings, C.V. Jakubzick, P.M. Henson, W. J. Janssen, Deletion of c-FLIP from CD11bhi macrophages prevents development of bleomycin-induced lung fibrosis, Am. J. Respir. Cell Mol. Biol. 58 (2018) 66–78, https://doi.org/10.1165/rcmb.2017-0154OC.

[55] EY Bissonnette, JF Lauzon-Joset, JS Debley, SF Ziegler, Cross-Talk Between Alveolar Macrophages and Lung Epithelial Cells is Essential to Maintain Lung Homeostasis, Front Immunol 11 (2020) 583042, https://doi.org/10.3389/fimmu.2020.583042.

[56] H Tao, Y Xu, S Zhang, The Role of Macrophages and Alveolar Epithelial Cells in the Development of ARDS, Inflammation 46 (2023) 47–55, https://doi.org/10.1007/s10753-022-01726-w.

[57] V Mysore, X Cullere, J Mears, F Rosetti, K Okubo, PX Liew, et al., FcγR engagement reprograms neutrophils into antigen cross-presenting cells that elicit acquired anti-tumor immunity, Nat Commun 12 (2021) 4791, https://doi.org/10.1038/s41467-021-24591-x.

[58] M Rambault, FB Gilbert, P Roussel, A Tessier, V David, P Germon, et al., Neutrophils expressing major histocompatibility complex class II molecules circulate in blood and milk during mastitis and show high microbicidal activity, J Dairy Sci 106 (2023) 4245–4256, https://doi.org/10.3168/jds.2022-22728.

[59] SM Meinderts, G Baker, S van Wijk, BM Beuger, J Geissler, MH Jansen, et al., Neutrophils acquire antigen-presenting cell features after phagocytosis of IgG-opsonized erythrocytes, Blood Adv 3 (2019) 1761–1773, https://doi.org/10.1182/bloodadvances.2018028753.

[60] C. Nathan, A. Ding, Nonresolving inflammation, Cell. 140 (2010) 871–882, https://doi.org/10.1016/j.cell.2010.02.029.

[61] P.J. Murray, T.A. Wynn, Protective and pathogenic functions of macrophage subsets, Nat. Rev. Immunol. 11 (2011) 723–737, https://doi.org/10.1038/nri3073.

[62] F. Geissmann, S. Jung, D.R. Littman, Blood monocytes consist of two principal subsets with distinct migratory properties, Immunity 19 (2003) 71–82, https://doi.org/10.1016/S1074-7613(03)00174-2.

[63] F. Ginhoux, S. Jung, Monocytes and macrophages: developmental pathways and tissue homeostasis, Nat. Rev. Immunol. 14 (2014) 392–404, https://doi.org/10.1038/nri3671.

[64] A. Biswas, D. Bruder, S.A. Wolf, A. Jeron, M. Mack, M.M. Heimesaat, I.R. Dunay, Ly6Chigh monocytes control cerebral toxoplasmosis, J. Immunol. 194 (2015) 3223–3235, https://doi.org/10.4049/jimmunol.1402037.

[65] L. Möhle, N. Israel, K. Paarmann, M. Krohn, S. Pietkiewicz, A. Müller, I.N. Lavrik, J.S. Buguliskis, B.H. Schott, D. Schlüter, E.D. Gundelfinger, D. Montag, U. Seifert, J. Pahnke, I.R. Dunay, Chronic Toxoplasma gondii infection enhances β-amyloid phagocytosis and clearance by recruited monocytes, Acta Neuropathol. Commun 4 (2016) 25, https://doi.org/10.1186/s40478-016-0293-8.

[66] RMM Brito, MCM Silva, F Vieira-Santos, C Almeida Lopes, JLN Souza, AL Bastilho, et al., Chronic infection by atypical *Toxoplasma gondii* strain induces disturbance in microglia population and altered behaviour in mice, Brain Behav Immun Health 30 (2023) 100652, https://doi.org/10.1016/j.bbih.2023.100652.

[67] S. Heyde, L. Philipsen, P. Formaglio, Y. Fu, I. Baars, G. Höbbel, C.L. Kleinholz, E.A. Seiß, J. Stettin, P. Gintschel, A. Dudeck, P. Bousso, B. Schraven, A.J. Müller, CD11c-expressing Ly6C+CCR2+ monocytes constitute a reservoir for efficient Leishmania proliferation and cell-to-cell transmission, PLoS Pathog. 14 (2018) 1–30, https://doi.org/10.1371/journal.ppat.1007374.

[68] P.D. Fromm, J. Kling, M. Mack, J.D. Sedgwick, H. Körner, Loss of TNF signaling facilitates the development of a novel Ly-6Clow macrophage population permissive for Leishmania major infection, J. Immunol. 188 (2012) 6258–6266, https://doi.org/10.4049/jimmunol.1100977.

[69] N.M. Girgis, U.M. Gundra, L.N. Ward, M. Cabrera, U. Frevert, P. Loke, Ly6Chigh monocytes become alternatively activated macrophages in schistosome granulomas with help from CD4+ cells, PLoS Pathog. 10 (2014), https://doi.org/10.1371/journal.ppat.1004080.

[70] L.A. Borthwick, L. Barron, K.M. Hart, K.M. Vannella, R.W. Thompson, S. Oland, A. Cheever, J. Sciurba, T.R. Ramalingam, A.J. Fisher, T.A. Wynn, Macrophages are critical to the maintenance of IL-13-dependent lung inflammation and fibrosis, Mucosal Immunol. 9 (2016) 38–55, https://doi.org/10.1038/mi.2015.34.

[71] C.L.L. Chua, G. Brown, J.A. Hamilton, S. Rogerson, P. Boeuf, Monocytes and macrophages in malaria: protection or pathology? Trends Parasitol. 29 (2013) 26–34, https://doi.org/10.1016/j.pt.2012.10.002.

[72] J. Royo, A. Camara, B. Bertrand, P. Batigne, A. Coste, B. Pipy, A. Aubouy, Kinetics of monocyte subpopulations during experimental cerebral malaria and its resolution in a model of late chloroquine treatment, Front. Cell. Infect. Microbiol. 12 (2022) 1–12, https://doi.org/10.3389/fcimb.2022.952993.

[73] Caroline Junqueira, Camila R.R. Barbosa, Pedro A.C. Costa, T.-C. A, et al., Cytotoxic CD8+ T cells recognize and kill Plasmodium vivax- infected reticulocytes, Nat. Med. 176 (2018) 139–148, https://doi.org/10.4049/jimmunol.1801473.The.

[74] H. Possemiers, T.T. Pham, M. Coens, E. Pollenus, S. Knoops, S. Noppen, L. Vandermosten, S. D'haese, L. Dillemans, F. Prenen, D. Schols, B. Franke-Fayard, P. E. Van Den Steen, Skeleton binding protein-1-mediated parasite sequestration inhibits spontaneous resolution of malaria-associated acute respiratory distress syndrome, PLoS Pathog. 17 (2021), https://doi.org/10.1371/journal.ppat.1010114.

[75] A.P. et, al Otto, T.D. Böhme, U. Jackson, A comprehensive evaluation of rodent malaria parasite genomes and gene expression, PLoS Pathog. 12 (2014) 86, https://doi.org/10.1186/s12915-014-0086-0.

[76] L. Vandermosten, T.T. Pham, H. Possemiers, S. Knoops, E. Van Herck, J. Deckers, B. Franke-Fayard, T.J. Lamb, C.J. Janse, G. Opdenakker, P.E. Van Den Steen, Experimental malaria-associated acute respiratory distress syndrome is dependent on the parasite-host combination and coincides with normocyte invasion, Malar. J. 17 (2018) 1–17, https://doi.org/10.1186/s12936-018-2251-3.

[77] F.V.E.S. Castanheira, K.A. De Lima, G.C.M. Cebinelli, F. Sônego, A. Kanashiro, D.F. Colon, V. Borges, P.G. Czaikoski, J.M. Mota, T.M. Cunha, J.C. Alves-Filho, F. Y. Liew, F.Q. Cunha, CCR5-Positive inflammatory monocytes are crucial for control of sepsis, Shock 52 (2019) E100–E106, https://doi.org/10.1097/SHK.0000000000001301.

[78] R.S. Hotchkiss, L.L. Moldawer, S.M. Opal, K. Reinhart, I.R. Turnbull, J.L. Vincent, Sepsis and septic shock, Nat. Rev. Dis. Prim. 2 (2016), https://doi.org/10.1038/nrdp.2016.45.

[79] A. Chalkias, S. Aridas, D. Karageorgopoulos, G. Stratiotis, D. Mystrioti, A. Mallios, I. Nakos, N. Mpellos, A. Ganotopoulou, T. Xanthos, Severe sepsis and septic shock due to Plasmodium vivax infection, Am. J. Emerg. Med. 31 (2013) 761.e1–761.e2, https://doi.org/10.1016/j.ajem.2012.12.011.

[80] T. Njim, A. Dondorp, M. Mukaka, E.O. Ohuma, Identifying risk factors for the development of sepsis during adult severe malaria, Malar. J. 17 (2018) 1–10, https://doi.org/10.1186/s12936-018-2430-2.

[81] M.A. Auma, M.J. Siedner, D. Nyehangane, A. Nalusaji, M. Nakaye, J. Mwanga-Amumpaire, R. Muhindo, L.A. Wilson, Y. Boum, C.C. Moore, Malaria is an uncommon cause of adult sepsis in south-western Uganda, Malar. J. 12 (2013) 1–9, https://doi.org/10.1186/1475-2875-12-146.

[82] P. Tarigan, F. Ginting, Severe malaria vivax with sepsis bacterial: a case report, IOP Conf. Ser. Earth Environ. Sci. 125 (2018), https://doi.org/10.1088/1755-1315/125/1/012078.

[83] H. Gong, Y. Chen, M. Chen, J. Li, H. Zhang, S. Yan, C. Lv, Advanced development and mechanism of sepsis-related acute respiratory distress syndrome, Front. Med. 9 (2022), https://doi.org/10.3389/fmed.2022.1043859.

[84] B. Zhu, Y. Wu, S. Huang, R. Zhang, Y.M. Son, C. Li, I.S. Cheon, X. Gao, M. Wang, Y. Chen, X. Zhou, Q. Nguyen, A.T. Phan, S. Behl, M.M. Taketo, M. Mack, V. S. Shapiro, H. Zeng, H. Ebihara, J.J. Mullon, E.S. Edell, J.S. Reisenauer, N. Demirel, R.M. Kern, R. Chakraborty, W. Cui, M.H. Kaplan, X. Zhou, A.W. Goldrath, J. Sun, Uncoupling of macrophage inflammation from self-renewal modulates host recovery from respiratory viral infection, Immunity 54 (2021) 1200–1218.e9, https://doi.org/10.1016/j.immuni.2021.04.001.

[85] Y.M. Wang, X. Qi, F.C. Gong, Y. Chen, Z.T. Yang, E.Q. Mao, E.Z. Chen, Protective and predictive role of Mucin1 in sepsis-induced ALI/ARDS, Int. Immunopharm. 83 (2020) 106438, https://doi.org/10.1016/j.intimp.2020.106438.

[86] Y. Zhang, R. Lv, X. Hu, L. Jiang, D. Xiao, Y. Sun, J. Zhao, Q. Bao, J. Xie, The role of IL-33 on LPS-induced acute lung injury in mice, Inflammation 40 (2017) 285–294, https://doi.org/10.1007/s10753-016-0479-z.

[87] V. Fattori, L. Staurengo-Ferrari, T.H. Zaninelli, R. Casagrande, R.D. Oliveira, P. Louzada-Junior, T.M. Cunha, J.C. Alves-Filho, M.M. Teixeira, F.Q. Cunha, F. A. Amaral, W.A. Verri, IL-33 enhances macrophage release of IL-1β and promotes pain and inflammation in gouty arthritis, Inflamm. Res. 69 (2020) 1271–1282, https://doi.org/10.1007/s00011-020-01399-x.

[88] M.K. Tembhre, M.K. Sriwastva, M.P. Hote, S. Srivastava, P. Solanki, S. Imran, R. Lakshmy, A. Sharma, K. Jaiswal, A.D. Upadhyay, Interleukin-33 induces neutrophil extracellular trap (NET) formation and macrophage necroptosis via enhancing oxidative stress and secretion of proatherogenic factors in advanced atherosclerosis, Antioxidants 11 (2022) 1–15, https://doi.org/10.3390/antiox11122343.